Eur. Phys. J. E (2011) **34**: 45
DOI 10.1140/epje/i2011-11045-4

THE EUROPEAN PHYSICAL JOURNAL E

Regular Article

Compression of polyelectrolyte brushes in a salt-free theta solvent

M.W. Matsen[a]

School of Mathematical and Physical Sciences, University of Reading, Whiteknights, Reading RG6 6AX, UK

Received 13 January 2011 and Received in final form 25 February 2011
Published online: 10 May 2011 –

Abstract. This paper examines the normal force between two opposing polyelectrolyte brushes and the interpenetration of their chains that is responsible for sliding friction. It focuses on the special case of semi-dilute brushes in a salt-free theta solvent, for which Zhulina and Borisov (J. Chem. Phys. **107**, 5952 (1997)) have derived analytical predictions using the classical strong-stretching theory (SST). Interestingly, SST predicts that the brushes contract as they are compressed together maintaining a polymer-free gap, which provides an explanation for the ultra-low frictional forces observed in experiment. We examine the degree to which the SST predictions are affected by chain fluctuations by employing self-consistent field theory (SCFT). While the normal force is relatively unaffected, fluctuations are found to have a strong impact on brush interpenetration. Even still, the contraction of the brushes does significantly prolong the onset of interpenetration, implying that a sizeable normal force can be achieved before the sliding friction becomes significant.

1 Introduction

For some time now, surfaces coated with polymer brushes have been acknowledged for their ability to support large normal forces while still exhibiting low degrees of sliding friction. This can be understood from the classical strong-stretching theory (SST) [1–3]. In a good solvent, the polymer chains extend away from the grafting surface so as to maximize their interactions with the solvent, forming a parabolic concentration profile of height ℓ. When two opposing brushes are compressed together, the solvent is squeezed out causing a rise in free energy and thereby a repulsive normal force. According to SST, the brushes contract under compression avoiding any interpenetration, which accounts for the low sliding friction observed in experiment [4]. In reality, however, the thermal fluctuations ignored by the SST create a small tail in the concentration profile [5,6] extending beyond the classical brush height, ℓ, that leads to a small amount of interpenetration, which is understood to be the primary source of the friction [7–10]. The tails also have a significant effect on the normal force, mainly because they increase the effective height of the brushes. These fluctuation effects are readily accounted for by applying the numerical self-consistent field theory (SCFT) [11–13], which does indeed improve the theoretical agreement with experiment [14–18].

More recently, a further substantial reduction in sliding friction has been observed [19–22] for brushes composed of polyelectrolyte chains. However, understanding the reason for this is rather challenging due to the extra complexity of the system [23,24]. As well as the usual parameters controlling neutral brushes, such as grafting density, σ, the natural size of the polymer chains, $R_0 \equiv aN^{1/2}$, and the solvent quality specified by the excluded-volume parameter, v, polyelectrolyte brushes involve a number of additional parameters such as the number of charges per chain, N_c, and the electric permittivity of the solvent, ε. For strong polyelectrolytes, all the counter ions dissociate in solvent, but for weak polyelectrolytes, things are further complicated by the fact that the degree of dissociation is sensitive to, for example, the pH of the solvent. Furthermore, the solvent often contains extra ions from added salt. Fortunately, simple scaling theories [25–27] have been invaluable in helping navigate the extensive parameter space of polyelectrolyte brushes. This has also been supplemented by some useful SST [28–34] and SCFT [32–37] calculations as well as a number of simulations [38–41].

The natural starting point from which to develop our understanding is the simple reference system of semi-dilute brushes of strong polyelectrolyte chains in a salt-free theta solvent. In 1991, Pincus [25] used scaling arguments to show that the behavior of this system is governed by the single quantity, $\ell_B \sigma R_0 N_c^{3/2}$, where $\ell_B \equiv e^2/4\pi\epsilon k_B T$ is the Bjerrum length specifying the strength of the electrostatic interactions relative to the thermal energy. At large values of this parameter (the osmotic regime), the counter ions remain largely trapped inside the brush and the resulting osmotic pressure causes the brush height to increase as

[a] e-mail: m.w.matsen@reading.ac.uk

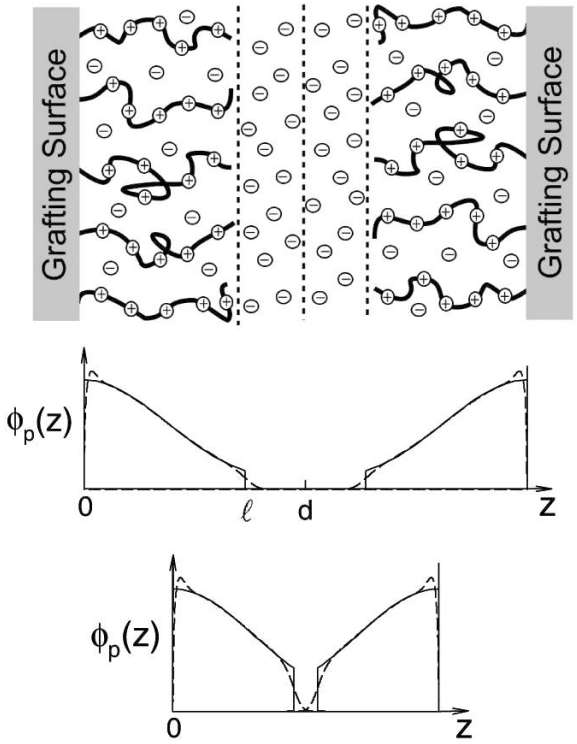

Fig. 1. Compression of two polyelectrolyte brushes. The concentration profiles, $\phi_p(z)$, predicted by SST (solid curves) exhibit a sharp cutoff at $z = \ell$ producing a polymer-free gap of width $2(d - \ell)$, whereas those of SCFT (dashed curves) include tails, leading to interpenetration as the separation, $2d$, becomes small.

$\ell \propto N_c^{1/2}$. For small values of the parameter (the Pincus regime), most of the ions escape the brush leading to a height that varies as $\ell \propto N_c^2$. While applications of SST to polyelectrolyte brushes generally require a number of supplementary approximations, Zhulina and Borisov [30] showed in 1997 that an exact analytical solution exists for this particular system. The solution nicely agrees with the scaling exponents predicted of Pincus, but since it originates from a full microscopic theory, it also provides the proportionality factors necessary for quantitative predictions. Furthermore, the calculation remains tractable for compressed brushes. Most interestingly, however, Zhulina and Borisov predicted that compressed brushes begin contracting prior to physical contact, as illustrated in fig. 1, maintaining a finite polymer-free gap as the normal force builds up. This provides a natural explanation for the ultra-low friction observed in the experiments [19–22].

Of course, the SST predictions will be altered by chain fluctuations, as is the case for neutral brushes. In particular, the tails of the brush profiles extending beyond the classical brush height, ℓ, will tend to close the gap between compressed brushes as illustrated in fig. 1. It has been suggested [20,30] that the size of the tails should be similar to that of neutral brushes. However, in neutral brushes, the self-consistent field predicted by SST exhibits a kink at $z = \ell$, whereas the field predicted by Zhulina and Borisov for polyelectrolyte brushes remains smooth. Consequently, the energy penalty for chains extending beyond $z = \ell$ is greatly reduced, and thus one should expect the tails to be much more significant. Here, we investigate the effect of chain fluctuations by solving the SCFT. Note that we employ the continuum version of Edwards [11] rather than the lattice version of Scheutjens and Fleer [12], because only the former can be applied to the exact same model used by the SST. This allows us to be certain that any differences between the SCFT and SST are entirely due to chain fluctuations.

2 Theory

Our study considers two opposing polyelectrolyte brushes with their grafting surfaces compressed to a separation of $2d$ (see fig. 1). Each brush has a uniform grafting density of $\sigma \equiv n_p/A$, where n_p is the number of grafted chains and A is the area of the grafting surface. The chains are taken to be monodisperse with a natural end-to-end length of $R_0 \equiv aN^{1/2}$, where N is the number of segments per chain and a is the statistical segment length. Each chain is given N_c ionic units distributed uniformly along its backbone, with all their counter ions dissociating in the background solvent (*i.e.*, a strong polyelectrolyte). The configuration of the α-th chain is specified by the space curve, $\mathbf{r}_{p,\alpha}(s)$, where s is a parameter that runs along the polymer backbone increasing from 0 at the free end to 1 at the grafted end. This allows us to define the dimensionless polymer concentration as

$$\hat{\phi}_p(\mathbf{r}) = \frac{N}{\rho_0} \sum_{\alpha=1}^{n_p} \int_0^1 \delta(\mathbf{r} - \mathbf{r}_{p,\alpha}(s))\mathrm{d}s, \tag{1}$$

where ρ_0 represents the segment density in a pure melt. Similarly, the position of the α-th counter ion is specified by the vector, $\mathbf{r}_{c,\alpha}$, such that the counter ion concentration can be expressed as

$$\hat{\phi}_c(\mathbf{r}) = \frac{1}{\rho_0} \sum_{\alpha=1}^{n_c} \delta(\mathbf{r} - \mathbf{r}_{c,\alpha}). \tag{2}$$

The charge density in the system is then specified as

$$\hat{\rho}(\mathbf{r}) = \frac{e\rho_0}{N} \left[N_c \hat{\phi}_p(\mathbf{r}) - N\hat{\phi}_c(\mathbf{r}) \right], \tag{3}$$

where we have assumed, without loss of generality, that the counter ions are negative and monovalent. Note that charge conservation requires $n_c = N_c n_p$. The electrostatic potential, $\hat{\psi}(\mathbf{r})$, created by the charge distribution must, of course, satisfy the Maxwell equation

$$-\epsilon \nabla^2 \hat{\psi}(\mathbf{r}) = \hat{\rho}(\mathbf{r}). \tag{4}$$

A full statistical mechanical treatment of this system is intractable, and so we implement SCFT. The general SCFT for polyelectrolytes was introduced some time ago [42,43], and there has since been several applications

to brushes [35–37]. However, we introduce several improvements to increase the accuracy and efficiency of our SCFT calculations, and for comparison purposes we also present the SST [30] in parallel with the SCFT.

The mean-field approximation replaces the molecular interactions by an effective field, $w(\mathbf{r})$. With that, the energy, E, of a single polymer becomes

$$\frac{E[\mathbf{r}_p]}{k_BT} = \int_0^1 \left[\frac{3}{2R_0^2}|\mathbf{r}_p'(s)|^2 + w(\mathbf{r}_p(s))\right] \mathrm{d}s, \tag{5}$$

where $w(z)$ is related to the ensemble-averaged polymer concentration, $\phi_p(z) \equiv \langle\hat{\phi}_p(\mathbf{r})\rangle$, and electric potential, $\psi(z) \equiv \langle\hat{\psi}(\mathbf{r})\rangle$, by the self-consistent condition

$$w(z) = vN\phi_p(z) + eN_c\psi(z)/k_BT. \tag{6}$$

This assumes that there is sufficient overlap between the polymers that the ensemble averages have no significant lateral dependence on x and y. For further simplicity, we now restrict our attention to theta solvents, for which $v = 0$.

One of our improvements is to remove the irrelevant parameters by switching to the scaled the quantities

$$Z \equiv z/R_0, \tag{7}$$
$$D \equiv d/R_0, \tag{8}$$
$$L_B \equiv 4\pi\ell_B\sigma R_0, \tag{9}$$
$$\Psi(Z) \equiv e\psi(z)/k_BT, \tag{10}$$
$$\Phi_p(Z) \equiv a^2\rho_0\phi_p(z)/\sigma R_0, \tag{11}$$
$$\Phi_c(Z) \equiv \rho_0 R_0\phi_c(z)/\sigma N_c. \tag{12}$$

This leaves just three reduced system parameters, L_B, N_c, and D, which effectively control the grafting density, charge per polymer, and separation of the brushes, respectively. In terms of the scaled quantities, the Maxwell equation (4), which is generally referred to as the Poisson-Boltzmann equation, becomes

$$\Psi''(Z) = -L_BN_c[\Phi_p(Z) - \Phi_c(Z)]. \tag{13}$$

Another improvement is to take advantage of the fact that the polymer concentration has a limited range, $\ell \equiv LR_0$, beyond which the polymer profile becomes negligible. (We require L to be large enough that $\Phi_p(L)N_c^{1/2} < 10^{-9}$.) This allows us to break the system into an inner region, $0 < Z < L$, containing the polymer chains that is solved numerically, and an outer region, $L < Z < D$, that is solved analytically. This strategy is also used in the SST derivation, where in that case L corresponds to the classical brush height.

To proceed, we need boundary conditions for the Poisson-Boltzmann equation. Integrating eq. (13) gives

$$\Psi'(Z) = -L_BN_c\int_{-\infty}^{Z}[\Phi_p(Z') - \Phi_c(Z')]\,\mathrm{d}Z', \tag{14}$$

from which it follows that

$$\Psi'(0) = 0, \tag{15}$$
$$\Psi'(L) = -L_BN_c(1 - f_c), \tag{16}$$
$$\Psi'(D) = 0, \tag{17}$$

where

$$f_c \equiv \int_0^L \Phi_c(Z)\mathrm{d}Z \tag{18}$$

specifies the fraction of counter ions remaining inside the brush. The solution for the potential still involves an arbitrary constant of integration, which allows us to set $\Psi(L) = 0$.

The counter ion distribution can then be split into

$$\Phi_c(Z) = \frac{f_c\exp(\Psi(Z))}{\int_0^L\exp(\Psi(Z))\mathrm{d}Z}, \quad \text{for } Z \le L, \tag{19}$$

and

$$\Phi_c(Z) = \frac{(1-f_c)\exp(\Psi(Z))}{\int_L^D\exp(\Psi(Z))\mathrm{d}Z}, \quad \text{for } Z \ge L. \tag{20}$$

Continuity at $Z = L$ requires

$$\frac{1-f_c}{f_c} = \frac{\int_L^D\exp(\Psi(Z))\mathrm{d}Z}{\int_0^L\exp(\Psi(Z))\mathrm{d}Z}. \tag{21}$$

2.1 Outside the brush

In the outer region, eq. (13) is solved with $\Phi_p(Z) = 0$ and the boundary conditions, eqs. (16) and (17). To simplify things, we scale the spatial quantities as $\bar{Z} = 2Z/\Lambda_{\mathrm{GC}}$, where

$$\Lambda_{\mathrm{GC}} \equiv \frac{2}{L_BN_c(1-f_c)} \tag{22}$$

is a dimensionless Guoy-Chapman length. This reduces the equations to

$$\bar{\Psi}''(\bar{Z}) = \frac{\exp(\bar{\Psi}(\bar{Z}))}{\int_{\bar{L}}^{\bar{D}}\exp(\bar{\Psi}(\bar{Z}))\mathrm{d}\bar{Z}}, \tag{23}$$
$$\bar{\Psi}'(\bar{L}) = -1, \tag{24}$$
$$\bar{\Psi}'(\bar{D}) = 0. \tag{25}$$

Multiplying by $\bar{\Psi}'(\bar{Z})$ and integrating between $\bar{Z}$ and $\bar{D}$ gives

$$\frac{1}{2}[\bar{\Psi}'(\bar{Z})]^2 = \frac{\exp(\bar{\Psi}(\bar{Z})) - \exp(\bar{\Psi}(\bar{D}))}{\int_{\bar{L}}^{\bar{D}}\exp(\bar{\Psi}(\bar{Z}))\mathrm{d}\bar{Z}}. \tag{26}$$

Then integrating $\bar{\Psi}'(\bar{Z})$ and returning to the unbarred quantities provides the solution,

$$\Psi(Z) = \Psi(D) - 2\ln\left[\cos\left(\frac{D-Z}{\Lambda_{\mathrm{GC}}\sqrt{\exp(-\Psi(D))-1}}\right)\right], \tag{27}$$

where $\Psi(D)$ is determined by solving

$$\exp(\Psi(D)/2) = \cos\left(\frac{D-L}{\Lambda_{\mathrm{GC}}\sqrt{\exp(-\Psi(D))-1}}\right). \tag{28}$$

To solve the inner part of the problem, we will need the integral

$$\int_L^D \exp(\Psi(Z))\mathrm{d}Z = \Gamma\Lambda_{\mathrm{CG}}, \tag{29}$$

where

$$\Gamma \equiv 1 - \exp(\Psi(D)) \tag{30}$$

is a quantity that decreases from 1 to 0 as the brush is compressed. With that, the condition in eq. (21) can be rewritten as

$$\frac{1-f_c}{f_c} = \frac{\Gamma\Lambda_{\mathrm{CG}}}{\int_0^L \exp(\Psi(Z))\mathrm{d}Z}\,. \tag{31}$$

2.2 SST treatment of the brush

Zhulina and Borisov [30] solved the SST by the method of Semenov [1] whereby the field, $w(z)$, emerges by minimizing the free energy. Here we follow a simplified approach, where an analogy with classical mechanics identified by Milner, Witten and Cates [2] allows us to immediately deduce the parabolic shape of the field [28–34],

$$w(z) = \frac{3\pi^2}{8R_0^2}(\ell^2 - z^2), \tag{32}$$

inside the brush. For the case of a theta solvent (*i.e.*, $v = 0$), it follows that

$$\Psi(Z) = \frac{3\pi^2}{8N_c}(L^2 - Z^2). \tag{33}$$

From this, eq. (13) leads us to the result

$$\Phi_p(Z) = \Phi_c(Z) + \frac{3\pi^2}{4L_B N_c^2}\,, \tag{34}$$

which implies that

$$1 - f_c = \int_0^L [\Phi_p(Z) - \Phi_c(Z)]\mathrm{d}Z = \frac{3\pi^2 L}{4L_B N_c^2}\,. \tag{35}$$

Combining eqs. (19), (21), (29) and (33), the counter ion concentration inside the brush can be expressed as

$$\Phi_c(Z) = \frac{1}{\mathcal{Q}_c N_c^{1/2}} \exp\left(\frac{3\pi^2}{8N_c}(L^2 - Z^2)\right), \tag{36}$$

where

$$\mathcal{Q}_c \equiv \frac{1}{N_c^{1/2}} \int_0^D \exp(\Psi_c(Z))\mathrm{d}Z = \frac{\Gamma\Lambda_{\mathrm{GC}}}{(1-f_c)N_c^{1/2}}\,. \tag{37}$$

So that the inner solution of $\Phi_c(Z)$ matches the outer solution, we need to satisfy eq. (31). By inserting eq. (33) and making use of eq. (35), this requirement reduces to

$$\frac{1-f_c}{f_c} = \frac{\Gamma}{g(3\pi^2 L^2/8N_c)}\,, \tag{38}$$

where we have defined

$$g(y) \equiv y \int_0^1 \exp(y(1-x^2))\mathrm{d}x. \tag{39}$$

Careful inspection of the SST equations reveals that N_c can be scaled out of the problem by dividing all lengths by $N_c^{1/2}$ while multiplying all concentrations by $N_c^{1/2}$. As such, a solution to the SST equations is obtained analytically by selecting values for $L/N_c^{1/2}$ and $0 < \Gamma < 1$. From these values, $\exp(\Psi(D))$ is evaluated using eq. (30), and then $D/N_c^{1/2}$ is calculated from eq. (28). Next f_c is obtained from eq. (38), followed by $L_B N_c^{3/2}$ from eq. (35). Equation (22) then provides $\Lambda_{\mathrm{GC}}/N_c^{1/2}$ from which we obtain Q_c using eq. (37). With that, we can evaluate $\phi_c(Z)N_c^{1/2}$ using eq. (36) and then $\phi_p(Z)N_c^{1/2}$ using eq. (34).

Of course, it is more natural to work with the independent variables, $L_B N_c^{3/2}$ and $D/N_c^{1/2}$, rather than the dependent quantities, $L/N_c^{1/2}$ and Γ. This is easily done by using a simple Newton-Raphson iteration to adjust $L/N_c^{1/2}$ and Γ so as to achieve the desired values of $L_B N_c^{3/2}$ and $D/N_c^{1/2}$.

2.3 SCFT treatment of the brush

In the SCFT [6], the polymer concentration is given by

$$\Phi_p(Z) = \frac{1}{q(\Delta,1)} \int_0^1 q(Z,s)q^\dagger(Z,s)\mathrm{d}s, \tag{40}$$

where $q(Z,s)$ satisfies the modified diffusion equation

$$\frac{\partial}{\partial s}q(Z,s) = \left[\frac{1}{6}\frac{\partial^2}{\partial Z^2} - w(Z)\right]q(Z,s), \tag{41}$$

subject to the initial condition, $q(Z,0) = 1$. So as to prevent the polymers from penetrating the grafting surface, the diffusion equation is solved with the Dirichlet boundary condition at $Z = 0$ [44]. When $L = D$, the Neumann boundary condition is used at $Z = L$ since this then corresponds to a plane of mirror reflection (see fig. 1). We continue to use the Neumann boundary when $L < D$, although the choice of boundary condition becomes immaterial since $\Phi_p(L) \approx 0$. Similarly, $q^\dagger(Z,s)$ satisfies an analogous diffusion equation, but with the right-hand side multiplied by -1. It is also solved with the same boundary conditions, but subject to the condition, $q^\dagger(Z,1) = \delta(Z - \Delta)$, where Δ is a small positive number. We use a value of $\Delta \approx 10^{-4}$.

Unlike in SST, N_c cannot be scaled out of the problem, and so there remain three separate system parameters, N_c, L_B and D. For a given set of values, a numerical solution of SCFT begins with an initial guess for $w(Z)$ in the interval, $0 \le Z \le L$. For this, we use either the SST solution or a previous SCFT solution obtained for a neighboring set of parameter values. Next the diffusion eq. (41) is solved

on a discrete mesh by the standard Crank-Nicolson algorithm [6]. Once $\Phi_p(z)$ has been evaluated, $\Psi(Z)$ is determined by solving the Poisson-Boltzmann equation (13) using the Newton-Raphson algorithm. To increase the speed, we approximate the Jacobian by a tridiagonal matrix by ignoring the dependence on $\Psi(Z)$ in the denominator of eq. (19) for $\Phi_c(Z)$.

Next the field is adjusted to satisfy $w(Z) = N_c\,\Psi(Z)$, using the Anderson-mixing scheme [45]. Convergence is generally achieved within just 20 iterations. If $L = D$ then the fraction of the counter ions remaining in the brush, f_c, is simply set to one, but otherwise f_c is adjusted by a Newton-Raphson iteration so as to satisfy eq. (31). Even though we use a very fine mesh in order to achieve high precision (*e.g.*, 5000 points along the chain contour and 4000 spatial points for $0 < Z < L$), a self-consistent solution takes less than a minute to evaluate on a single computer processor.

Once the self-consistent field, $w(Z)$, is known, we can determine the level of interpenetration between the two brushes. This is done by reflecting $w(Z)$ about the midplane, $Z = D$, and solving the diffusion eq. (41) in the full interval, $0 \le Z \le 2D$, with the same initial conditions. The resulting concentration profile, $\Phi_{p0}(Z)$, is then that of a single brush grafted to $Z = \Delta$. From that, we define the degree of interpenetration by the integral

$$\Sigma_p = \int_D^{2D} \Phi_{p0}(Z)\mathrm{d}Z. \tag{42}$$

2.4 Free energy

The free energy of the polyelectrolyte brush, $F = F_p + F_c + F_e$, is conveniently divided into three parts. The electrostatic energy is

$$\frac{F_e}{n_c k_B T} = \frac{1}{2}\int_0^D \Psi(Z)[\Phi_p(Z) - \Phi_c(Z)]\mathrm{d}Z, \tag{43}$$

$$= \frac{1}{3}(1-f_c)\Psi(0) - (D-L)\Phi_c(D) + 1 - f_c. \tag{44}$$

The first term in eq. (44) comes from integrating inside the brush and follows immediately from eqs. (33) and (34), while the calculation outside the brush is performed as

$$\int_L^D \Psi(Z)\Phi_c(Z)\mathrm{d}Z = \frac{1}{L_B N_c}\int_L^D \Psi(Z)\Psi''(Z)\mathrm{d}Z, \tag{45}$$

$$= -\frac{1}{L_B N_c}\int_L^D [\Psi'(Z)]^2\mathrm{d}Z, \tag{46}$$

$$= 2\int_L^D [\Phi_c(D) - \Phi_c(Z)]\mathrm{d}Z, \tag{47}$$

using the Poisson-Boltzmann equation (13) followed with integration by parts and then the identity from eq. (26).

The translational entropy of the counter ions is given by

$$\frac{F_c}{n_c k_B T} = \int_0^D \Phi_c(Z)\ln[\Phi_c(Z)N_c^{1/2}]\mathrm{d}Z, \tag{48}$$

$$= -\ln\mathcal{Q}_c + \int_0^D \Phi_c(Z)\Psi(Z)\mathrm{d}Z. \tag{49}$$

For convenience, we include $N_c^{1/2}$ in the logarithm of eq. (48), which simply adds an irrelevant constant to the free energy. The equivalence of the resulting expression to eq. (49) follows from the fact that $\ln[\Phi_c(Z)N_c^{1/2}] = \Psi(Z) - \ln\mathcal{Q}_c$.

The expression for the free energy of the polymer chains differs for the two theories. In SST, it is given by

$$\frac{F_p}{n_c k_B T} = \frac{3\pi^2}{8N_c}\int_0^L Z^2\Phi_p(Z)\mathrm{d}Z, \tag{50}$$

$$= \Psi(0) - \int_0^L \Phi_p(Z)\Psi(Z)\mathrm{d}Z. \tag{51}$$

Equation (50) comes from the well-known expression developed by Milner, Witten and Cates, and the equivalence to eq. (51) is an immediate consequence of the fact that $Z^2 \propto \Psi(0) - \Psi(Z)$. In SCFT [6], the entropic stretching energy of the brush is

$$\frac{F_p}{n_c k_B T} = -\frac{1}{N_c}\ln q(\Delta, 1) - \int_0^L \Phi_p(Z)\Psi(Z)\mathrm{d}Z. \tag{52}$$

Some care has to be taken though. The free energy is sensitive to the small separation, Δ, between the substrate and the grafting plane [6]. Therefore, it is important that Δ remains fixed as the brush is compressed so that its effect cancels out when we compute free energy differences, ΔF.

3 Results

We now compare the SST and SCFT predictions, starting with an isolated brush and finishing with two compressed brushes. Since both theories are implemented for the exact same underlying model, we can be certain that the differences are entirely attributable to chain fluctuations.

3.1 Isolated brush

We begin by examining an isolated brush with SST (*i.e.*, $D \to \infty$ for which $\Gamma = 1$), where the behavior is controlled by the single quantity, $L_B N_c^{3/2}$ [46]. Figure 2 plots the fraction of counter ions in the brush, f_c, and the classical brush height, L. In the Pincus regime ($L_B N_c^{3/2} \ll 1$), the fraction of counter ions remaining in the brush scales as

$$f_c \approx \frac{2L_B^2 N_c^3}{3\pi^2}, \tag{53}$$

which is obtained using the approximations, $1 - f_c \approx 1$ and $g(y) \approx y$, in eq. (38). From that, the scaling of the brush height

$$L \approx \frac{4L_B N_c^2}{3\pi^2}, \tag{54}$$

follows from eq. (35). In the osmotic regime ($L_B N_c^{3/2} \gg 1$), f_c saturates to one, and the extension of the brush is approximately

$$L \approx \frac{4L_B N_c^2}{3\pi^2 g(3\pi^2 L^2/8N_c)}, \tag{55}$$

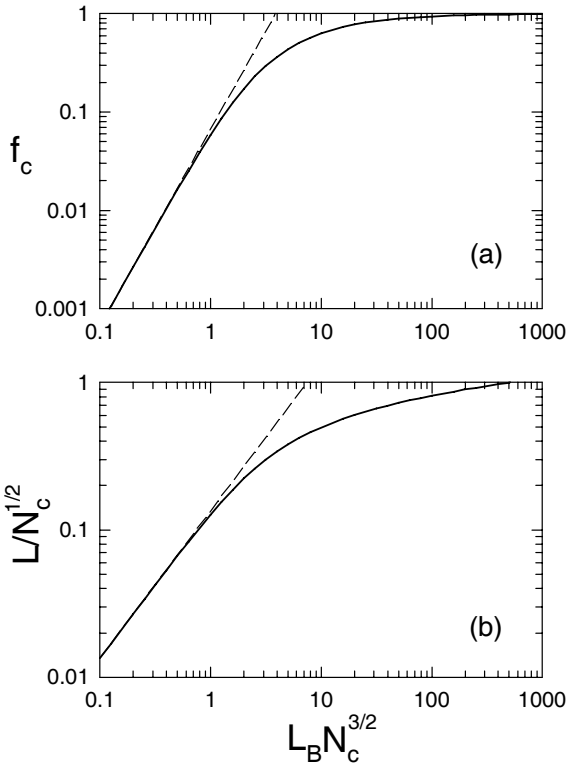

Fig. 2. SST results for an isolated brush showing (a) the fraction of counter ions confined to the brush, f_c, and (b) the classical brush height, L. Dashed lines denote the power law approximations in eqs. (53) and (54) for the Pincus regime. Note that (b) is analogous to curve 1 in fig. 2 of ref. [30].

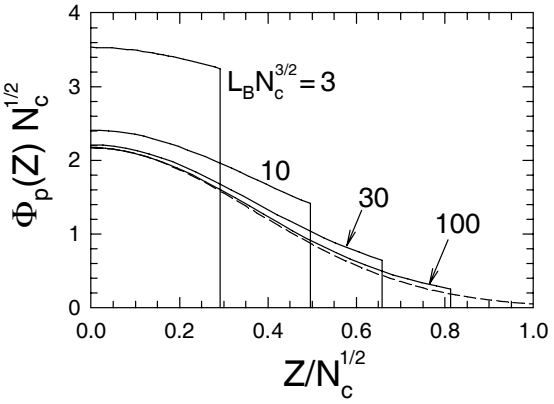

Fig. 3. Concentration profiles of an isolated brush calculated from SST, analogous to fig. 8 from ref. [30]. The dashed curve shows the Gaussian distribution in eq. (57).

where $g(y) \approx \sqrt{\pi y}\exp(y)/2$. In this case, L does not follow a power law behavior.

Figure 3 shows the brush profile, $\Phi_p(Z)$, at several different values of $L_B N_c^{3/2}$. According to eqs. (34) and (36), the profile is equal to a constant plus a truncated Gaussian. In the Pincus regime, where the constant part dominates,

$$\Phi_p(Z) \approx \frac{3\pi^2}{4L_B N_c^2}\,, \tag{56}$$

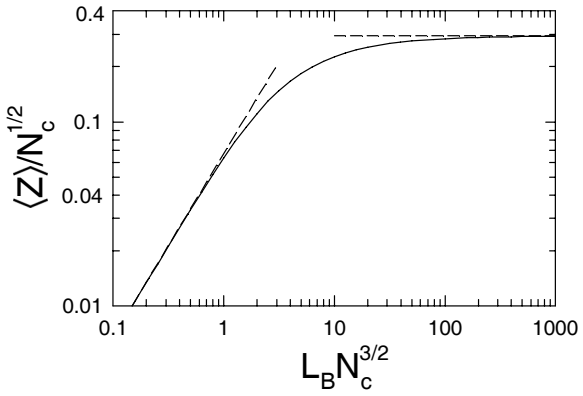

Fig. 4. Average height of an isolated brush as calculated from SST, analogous to curve 2 in fig. 2 of ref. [30]. Dashed lines show the asymptotic approximates from eqs. (58) and (59).

for $Z \le L$, while in the osmotic regime, the profile approaches

$$\Phi_p(Z) \approx \sqrt{\frac{3\pi}{2N_c}}\exp\left(-\frac{3\pi^2 Z^2}{8N_c}\right). \tag{57}$$

We can see from fig. 3 that, in the osmotic regime, L does not represent a meaningful measure of the brush height. A more appropriate measure is the first moment, $\langle Z\rangle$, of the $\Phi_p(Z)$ distribution, plotted in fig. 4. The asymptotic value in the Pincus regime,

$$\langle Z\rangle \approx \frac{2L_B N_c^2}{3\pi^2}\,, \tag{58}$$

follows directly from eq. (56), while the asymptotic limit in the osmotic regime,

$$\langle Z\rangle \approx \left(\frac{8N_c}{3\pi^3}\right)^{1/2}, \tag{59}$$

is obtained using eq. (57). This time both limits obey power law behaviors.

We now compare SCFT to SST in fig. 5a to examine the effect of chain fluctuations. Just as for neutral brushes [6], fluctuations have two main effects. Firstly, they cause a depletion zone next to the substrate, and secondly, they create a tail that extends beyond the SST value of L. Nevertheless, the SCFT profiles match the SST predictions well for intermediate values of Z, although much less so for the smaller value of $L_B N_c^{3/2} = 10$, where the chain fluctuations are far stronger.

In appendix A, we show that the energy, ΔE, required to pull a single chain end a distance h beyond the end of the brush, $z = \ell$, scales as

$$\frac{\Delta E}{k_B T} \approx \frac{2^{7/2}}{15\pi}\left(\frac{h}{\xi}\right)^{5/2}, \tag{60}$$

where the characteristic height,

$$\xi \equiv \Xi R_0 = \frac{L^{1/5} R_0}{(L_B N_c^2 \Phi_p(L))^{2/5}}\,, \tag{61}$$

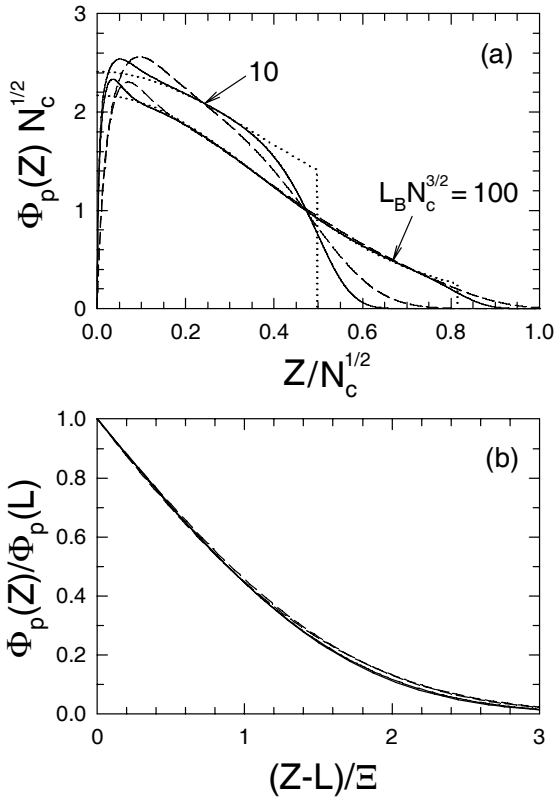

Fig. 5. (a) Profiles of an isolated brush calculated with SCFT for $N_c = 25$ (dashed curves) and $N_c = 100$ (solid curves), compared to the SST predictions (dotted curves) from fig. 3. (b) Tail region beyond the classical brush height, $z > \ell$, scaled with respect to ξ from eq. (61).

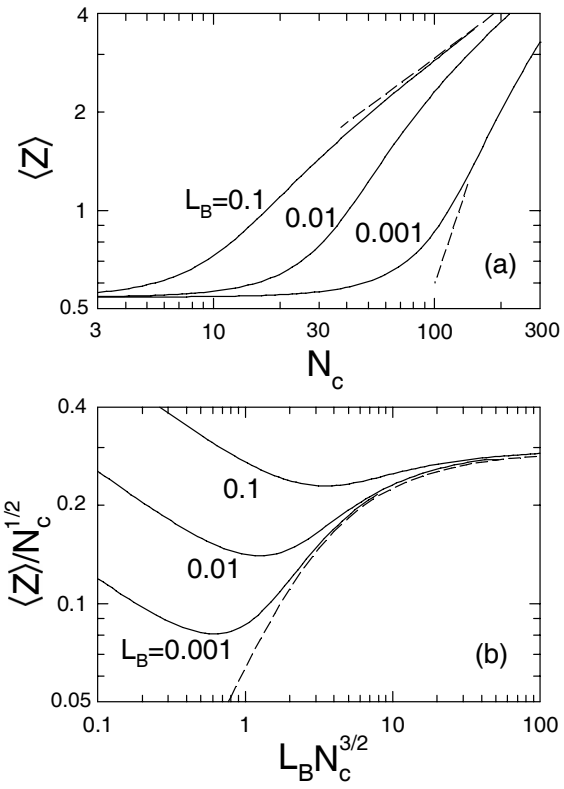

Fig. 6. (a) Average height of an isolated brush calculated from SCFT as a function of N_c for various values of L_B. Dashed lines denote the expected scaling of $\langle Z \rangle \sim N_c^{1/2}$ and $\sim N_c^2$ for the osmotic and Pincus regimes, respectively. (b) Comparison of the SCFT results (solid curves) with the SST prediction (dashed curve) from fig. 4.

depends on the SST prediction for $\Phi_p(L)$. Figure 5b illustrates that the tails collapse onto a single master curve when the z axis is scaled with respect to ξ.

Figure 6a shows how the average brush height, $\langle Z \rangle$, varies with N_c for different values of L_B. The upper and lower dashed lines denote the $\langle Z \rangle \sim N_c^{1/2}$ and $\langle Z \rangle \sim N_c^2$ scaling predicted by SST for the osmotic and Pincus regimes, respectively. While the former is realized for large L_B, the latter is never quite achieved even for our smallest choice of L_B. When we compare SCFT to SST in fig. 6b, we see that the SCFT results veer away from the SST prediction prior to the Pincus regime. The explanation is very simple. In SST, the brush height decreases to zero as the field acting on the polymers, $N_c\, \Psi(Z)$, vanishes. In SCFT, however, the chain fluctuations prevent the brush from completely collapsing; in the absence of a field, SCFT predicts $\langle Z \rangle = 0.543$, which indeed corresponds to the $N_c \to 0$ limit observed in fig. 6a.

3.2 Compressed brush

We now examine compressed brushes using SST. Figure 7 starts by showing the variation in f_c and L as $D \to 0$ for several values of $L_B N_c^{3/2}$ [46]. As the opposing brushes are compressed (see fig. 1), counter ions are forced back into the brush, which in turn causes the brush to contract, since $L \propto (1-f_c)$ according to eq. (35). Although the compression causes the gap between the brushes, $2(D-L)$, to monotonically decrease, the contraction remains sufficient to avoid physical contact between the brushes (*i.e.*, $L < D$). The SST does predict the gap to increase towards the Pincus regime ($L_B N_c^{3/2} \to 0$), but this is also where the chain fluctuations become more relevant.

Figure 8 compares the SST and SCFT profiles, $\Phi_{p0}(Z)$, under compression. Since the Pincus regime is swamped by fluctuation, we begin by examining the intermediate regime ($L_B N_c^{3/2} = 10$) for brushes with $N_c = 25$ (dashed curves) and $N_c = 100$ (solid curves) charges per polymer chain. Here the profiles have a large fluctuation-induced tail extending well beyond the classical profiles (dotted curves), particularly for the lower value of N_c. The bottom plot scales the tails with respect to ξ in eq. (61), showing that our prediction in appendix A for the characteristic range of the tail continues to hold for compressed brushes.

Figure 9 repeats the calculation for conditions just within the osmotic regime ($L_B N_c^{1/2} = 100$), where the fluctuations are considerably weaker as evident by the relatively smaller tails. As we can see from fig. 9b, the tails do not collapse nearly as well as in fig. 8b, when scaled with respect to ξ. The deviation from the master curve is

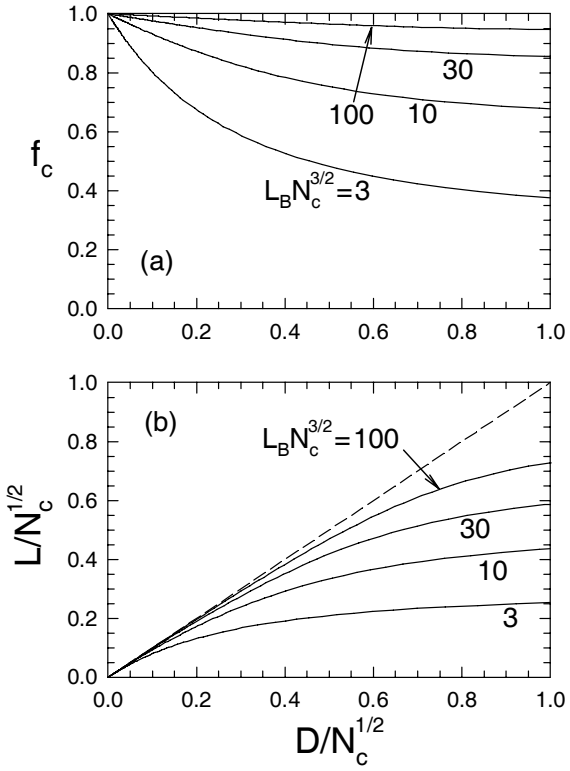

Fig. 7. SST results for a compressed brush showing (a) the fraction of counter ions confined to the brush, f_c, and (b) the classical brush height, L. The dashed line denotes $L = D$, corresponding to physical contact with the opposing brush. Note that (b) is analogous to fig. 7b in ref. [30].

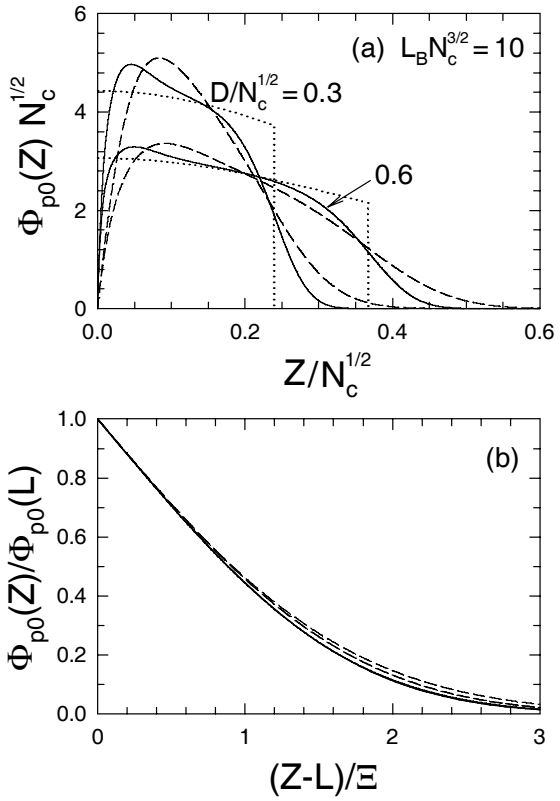

Fig. 8. Analogous to fig. 5, but for profiles of compressed brushes at $L_B N_c^{3/2} = 10$. The scaling plot (b) includes the four tails from (a) and two from the isolated brushes in fig. 5.

particular large for the case where $D = 2$ and $N_c = 25$. From fig. 9a, one can see that in this case most of the tail extends beyond $Z = D$, and thus penetrates into the opposing brush. In this limit where the gap between the brushes is small relative to the size of the tail, the characteristic range of the tail should revert back to the usual $\xi \propto \ell^{-1/3}$ scaling. Indeed, the alternative scaling plot in fig. 9c shows this to be true for sufficiently small D. Of course, this scaling will only persist so long as D is large enough that the brush is still strongly stretched.

To gauge the degree to which chain fluctuations affect the gap between compressed brushes predicted by SST, fig. 10 plots the amount of interpenetration, Σ_p, as a function of separation, $2D$ (see eq. (42)). Out of interest, we also calculate Σ_p using the uncompressed profiles in fig. 5a in order to assess how effective the contraction of the brushes is in preventing interpenetration. As we can see, the contraction allows D to decrease by an extra factor of two before physical contact occurs. Interestingly, the actual point of contact is quite similar for the two values of $L_B N_c^{3/2}$. Hence, the increased gap predicted by SST for small $L_B N_c^{3/2}$ is cancelled out by the larger fluctuation-induced tail in the brush profile.

The normal force between two opposing brushes is related to the free energy, $F(D) = F_p + F_c + F_e$, plotted in fig. 11 as a function of separation, $2D$. In the simple case of two flat parallel brushes, the force is just given by gradient of the free energy, $-F'(D)$. However, experiments [19,20] generally measure the force between crossed cylinders of radius R, which naturally involves a distribution of separations. Assuming the Derjaguin approximation [47] for $R \gg D$, the net force works out to be $2\pi\Delta F(D)/R$, where the free-energy difference, $\Delta F(D) = F(D) - F(\infty)$, is evaluated with D set to the minimum separation between the cylindrical surfaces.

Figure 11 compares the SST predictions (dotted curves) to those of SCFT for $N_c = 25$ (dashed curves) and $N_c = 100$ (solid curves). In the later case, where fluctuations are less significant, the SCFT results are almost indistinguishable from those of SST on the scale of the two plots. The elevated level of fluctuations at $N_c = 25$ does cause a slight increase in $\Delta F(D)$ at small D, which is primarily due the free energy of the brush, ΔF_p. Even still, the SST prediction is remarkably accurate, much more so than is the case for neutral brushes [18].

Thus, to a good approximation, the force curve is just a function of $L_B N_c^{3/2}$. We can also see that the main contribution to the force comes from the confinement of the counter ions, ΔF_c. In the intermediate regime examined in fig. 11a, the counter ion distribution still extends a considerable distance beyond the edge of the brush. Consequently, the repulsion between the brushes sets in well before the height of the isolated brush (denoted by the diamond symbols). For the osmotic region considered in

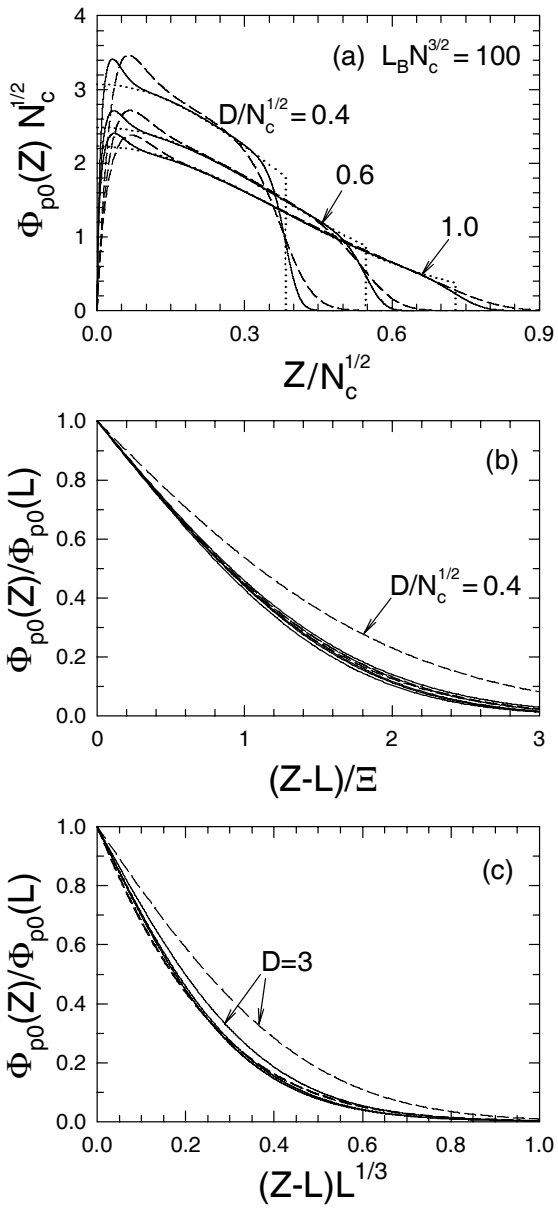

Fig. 9. Analogous to fig. 5, but for profiles of compressed brushes at $L_B N_c^{3/2} = 100$. The scaling plot (b) includes the four tails from (a) and two from the isolated brushes in fig. 5, while the other scaling plot (c) includes tails for compressions of $D = 1.5$, 2 and 3.

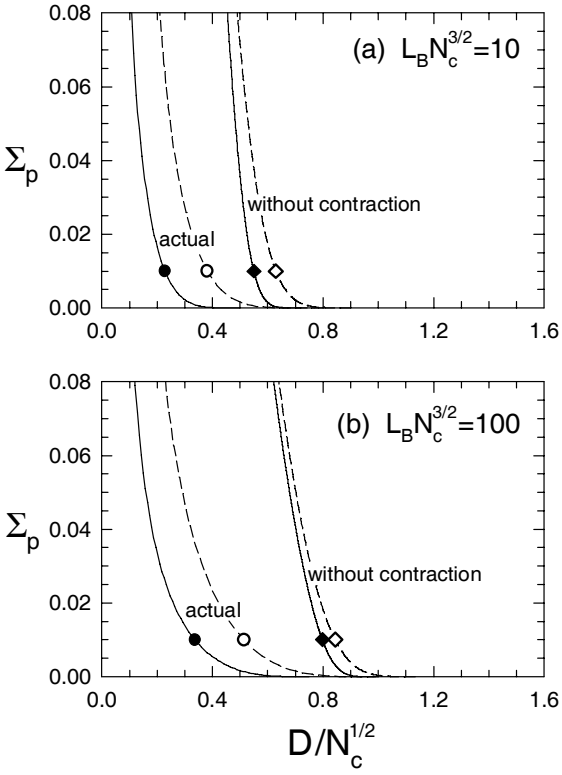

Fig. 10. Degree of interpenetration, Σ_p, between opposing brushes as a function of separation, $2d$, for (a) $L_B N_c^{3/2} = 10$ and (b) $L_B N_c^{3/2} = 100$, calculated with SCFT for $N_c = 25$ (dashed curves) and $N_c = 100$ (solid curves). To gauge the significance of the brush contraction, eq. (42) for Σ_p is evaluated with the actual profiles in fig. 8 as well as the profiles in fig. 5a prior to contraction.

fig. 11b, the counter ions are largely contained within the brush. Therefore, their confinement is not significantly affected until the brush begins contracting, and hence the force has a much shorter range.

4 Discussion

We should emphasize that our calculation makes a number of assumptions. For example, eq. (3) smears the positive charge of each polymer uniformly along its backbone, which is only valid for $N_c \gg 1$. It also assumes a strong polyelectrolyte, where all the counter ions dissociate from the polymer chains. The solvent degrees of freedom have been integrated out of the problem, which requires the brush to be dilute (*i.e.*, $\phi_p(0) \ll 1$) [6]. However, the brush must not be too dilute, because we also assume that the polymers overlap sufficiently for the brush to be treated as uniform in the lateral directions. Furthermore, the calculation requires the brush height, ℓ, to remain well below the fully extended length of a polymer, so that the Gaussian chain model remains valid.

The reason why opposing polyelectrolyte brushes contract prior to physical contact is very simple. As they come together, the counter ions are confined to an ever smaller region, which reduces their translational entropy as evident by the increase in their free energy (see ΔF_c in fig. 11). With this loss of entropy, some of the counter ions are pulled back into the brush (see f_c in fig. 7a) by the electrostatic attraction. Their presence in the brush then shields the charge on the polymer chains and reduces the electric field as confirmed by the drop in electrostatic energy (see ΔF_e in fig. 11). This then reduces the force on the chains, which allows them to contract and lower their stretching energy (see ΔF_p in fig. 11).

The analytical SST solution for polyelectrolyte brushes [30] is modified by the chain fluctuations in several

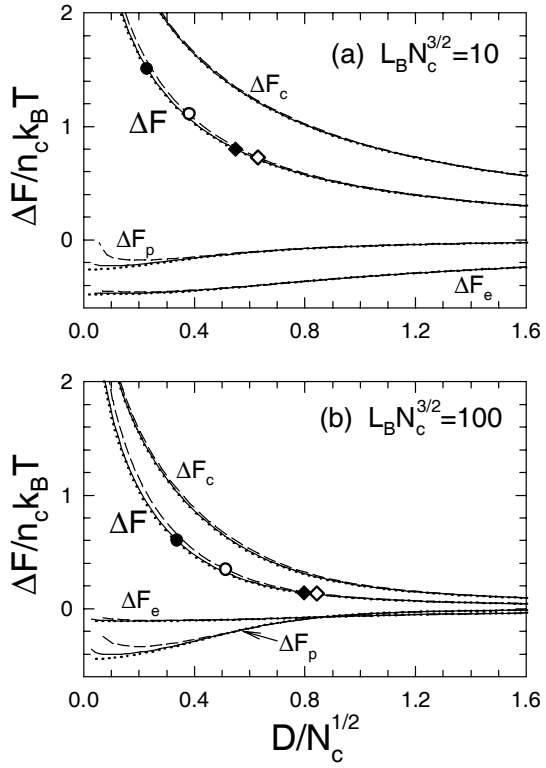

Fig. 11. Change in free energy, $\Delta F \equiv F(D) - F(\infty)$, of a compressed brush and its three contributions, ΔF_c, ΔF_p and ΔF_e, plotted as a function of compression for (a) $L_B N_c^{3/2} = 10$ and (b) $L_B N_c^{3/2} = 100$. SCFT results for $N_c = 25$ (dashed curves) and $N_c = 100$ (solid curves) are compared to the predictions of SST (dotted curves). The symbols correspond to the separations defined in fig. 10.

important ways. First of all, the thermal fluctuations prevent the brush from contracting below a thickness of order R_0, as illustrated in fig. 6a. According to fig. 6b, this obscures the Pincus regime unless $L_B \ll 10^{-3}$. When combined with the usual requirement $L_B N_c^{3/2} \lesssim 1$, it follows that the Pincus regime is only accessible for $N_c \gg 10^2$. This extends the similar conclusion by Israëls *et al.* [32] for brushes immersed in salt solutions.

In the osmotic regime, the most significant fluctuation effect is the tail at the extremity of the brush, which leads to the interpenetration responsible for shear forces. From SST, we know that the self-consistent field, $w(z)$, is approximately parabolic inside the brush, regardless of the particular system. For neutral brushes, $w(z)$ is proportional to $\phi_p(z)$. Thus $w(z) = 0$ for $z > \ell$ unless there is physical contact with an opposing brush in which case $w(z) = w(2\ell - z)$, assuming both brushes are identical. In either case, SST predicts a discontinuity in the slope of $w(z)$ at $z = \ell$, which results in a significant energy penalty for chains fluctuating beyond the classical brush height, ℓ. The result is a small tail extending a characteristic distance of $\xi \propto \ell^{-1/3}$ [5,6]. However, this is no longer the case for our polyelectrolyte brushes, because the field is proportional to $\psi(z)$ and thus remains smooth at $z = \ell$. Therefore it is much easier for chains to fluctuate beyond the classical brush height, ℓ, as illustrated in appendix A. This results in a longer tail, where the range scales as $\xi \propto \ell^{1/5}$. Furthermore, the amplitude of the tail will naturally be larger, because the blunt end of the brush profile predicted by SST (see fig. 3) implies a large segment concentration at $z = \ell$. Consequently, the fluctuation-induced tail is much more significant for polyelectrolyte brushes than for neutral brushes. The exception is when two opposing brushes come into physical contact, where the range of the tails exceeds the width of the polymer-free gap predicted by SST (see fig. 7). In this limit, the charge density of the ions inside the gap, which is proportional to $(1 - f_c)/(d - \ell)$, diverges producing a kink in the field at $z = d$. At this point, the range of the tail switches to the usual scaling law, $\xi \propto \ell^{-1/3}$ (see fig. 9c).

Table 1. Relative changes in the brush height, L, free energy, $\Delta F(L)$, and force, $-F'(L)$, at the point of physical contact (defined by $\Sigma_p = 0.01$) as a result of brush contraction, calculated for different values of L_B and N_c.

$L_B N_c^{3/2}$	N_c	L	$\Delta F(L)$	$-F'(L)$
10	25	0.61	1.5	2.1
10	100	0.42	1.9	3.3
100	25	0.61	2.6	4.0
100	100	0.42	4.3	7.1

We have not paid much attention to the depletion region predicted by SCFT at the grafting surface, because it should have little effect on the normal and shear forces, but it is nevertheless a significant fluctuation effect. The depletion region is well understood for neutral brushes [6], where its characteristic width is given by $\mu = R_0^2/\ell$. The physics of this regime will be the same for polyelectrolyte brushes, and thus its width will remain proportional to ℓ^{-1}. However, μ is affected by the distribution of chain tensions at the grafting surface, which in turn is proportional to the end-segment distribution. In neutral brushes, the shape of the end-segment distribution is unaffected by changes in ℓ, but this is no longer the case for polyelectrolyte brushes [30]. Thus μ will develop some dependence on L_B and N_c, as is the case for the height of the tail, ξ.

The contraction exhibited by polyelectrolyte brushes is highly significant because it allows the system to acquire a much larger normal force before the sliding friction sets in. This is illustrated quantitatively in table 1. From fig. 10, we see that the brushes contract to 61% and 42% of their unperturbed heights for $N_c = 25$ and 100, respectively, at the point where they come into physical contact (*i.e.*, $\Sigma_p = 0.01$). Interestingly, this is relatively insensitive to the value of $L_B N_c^{3/2}$, which implies that the increased polymer-free gap predicted by SST for smaller $L_B N_c^{3/2}$ (see fig. 7b) is negated by the increased size of the fluctuation-induced tail. Referring to fig. 11, the contraction translates into the relative increases in the free-energy difference, $\Delta F(L)$, and force, $-F'(L)$, listed in the forth and fifth columns of table 1, respectively. For our highly

charged ($N_c = 100$) osmotic brush ($L_B N_c^{3/2} = 100$), the contraction permits a seven-fold increase in the normal force between planar brushes (or a four-fold increase for crossed cylinders).

Experiments [48] also find that the low friction is retained when only one of the surfaces is coated with a polyelectrolyte brush. Indeed, the SST calculation remains identical if the midplane, $z = d$, is replaced by a hard wall. The brush still contracts as it is compressed so as to maintain a finite gap between the polymer chains and the wall. The SCFT calculation, however, does get modified slightly. The $z = d$ boundary condition for the diffusion eq. (41) is changed from the Neumann type corresponding to a plane of reflection symmetry to the Dirchlet type for an impenetrable surface. Nevertheless, this only has a very small effect on our SCFT results. In fact, there is a somewhat larger upturn in ΔF_p at high compression, leading to a slight increase in the normal force.

There still remain some significant questions to address, such as the effect of salt or solvent quantity on the gap between the brushes. Salt will screen the electrostatic interactions, which will suppress the long-range interaction predicted for the lower values of $L_B N_c^{3/2}$ (see fig. 11a) consistent with experiment [22]. Nevertheless, compression will still force counter ions back into the brush causing it to contract, and thus the polymer-free gap or low friction forces may still remain, which seems to be the case in experiment [19,20]. However, increasing the solvent quality ($v > 0$) will smooth the discontinuity in $\phi_p(z)$ predicted by SST, and thus would probably increase interpenetration and thus friction. Although this would seem to imply a benefit for reducing the solvent quality ($v < 0$), the consequence could be a discontinuous collapse of the brushes [26], which one may want to avoid. Extending our present study could help pinpoint the optimum brush parameters for producing large normal forces with minimal brush interpenetration.

5 Summary

This study examined the compression of semi-dilute polyelectrolyte brushes in a salt-free theta solvent, the case for which Zhulina and Borisov [30] derived an exact analytical solution to the classical SST. The SST predicts that for strongly stretched chains, the behavior depends only on a single parameter, $L_B N_c^{3/2}$, where N_c is the number of charges per chain and $L_B = 4\pi\ell_B\sigma R_0$ is a dimensionless Bjerrum length. Consistent with the scaling arguments of Pincus [25], there is an osmotic regime at $L_B N_c^{3/2} \gtrsim 100$ where most of the counter ions are trapped in the brush and a Pincus regime at $L_B N_c^{3/2} \lesssim 1$ where most of the ions escape. However one of the most interesting predictions emerging from the SST is that the brushes contract as they are compressed together so as to maintain a finite polymer-free gap. This mechanism, by which the brushes avoid physical contact, offers a potential explanation for how they can simultaneously maintain an ultra-low sliding friction with a large normal force [19–22].

The principle aim of our study was to use SCFT to investigate the degree to which these SST predictions, in particular the polymer-free gap, are affected by chain fluctuations. In SCFT, the behavior depends on L_B and N_c separately, with fluctuation effects becoming more pronounced as either quantity decreases. Although fluctuations have a negligible impact on the normal force predicted by SST, they do have a significant effect on the brush profile, $\phi_p(z)$. In fact, the fluctuations completely wipe out the Pincus regime unless the polymer chains are highly charged (*e.g.*, $N_c \gg 100$). In the osmotic regime, however, the polymer profiles predicted by SST remain largely unaffected, apart from a narrow depletion region next to the grafting surface and the emergence of a tail extending beyond the classical brush height, ℓ. The tail is analogous to that of neutral brushes, but generally with a larger amplitude, $\phi_p(\ell)$, and a longer range that scales as $\xi \propto \ell^{1/5}$ up to the point where the opposing brushes come into physical contact.

Although the tails promote interpenetration between brushes, the polymer-free gap predicted by SST does survive fluctuation effects long enough to have a very useful effect, particularly for large values of L_B and N_c. For the example in table 1 for $L_B = 0.1$ and $N_c = 100$, the gap survives until the brushes contract to about 40% of their unperturbed height, which is enough to allow the normal force between planar surfaces to increase by an extra seven-fold before the sliding friction begins to take effect. As we have discussed, these findings are certain to be affected by the addition of salt or variations in the solvent quality, but it remains to be seen to what degree this is the case.

This work was supported by EPSRC (EP/F068425/1).

Appendix A.

Here we calculate the energy, ΔE, required to pull a single chain-end a distance, h, beyond the edge of the brush, $z = \ell$, using SST. To do this, we first separate the chain into an exterior part, $0 \le s \le f$, and an interior part, $f \le s \le 1$. Inside the brush, the trajectory for the parabolic potential, eq. (6), is given by

$$z_p(s) = \ell \cos(\pi s/2)/\cos(\pi f/2). \tag{A.1}$$

The sudden drop in polymer concentration at the edge of the brush, $\Phi_p(L)$, causes a discontinuity in the second derivative of $w(z)$, and consequently the field immediately outside the brush is approximated by

$$w(z) = \frac{3\pi^2}{8R_0^2}[k^2(z-\ell)^2 - 2\ell(z-\ell)], \tag{A.2}$$

where

$$k^2 = \frac{4}{3\pi^2} L_B N_c^2 \Phi_p(L) - 1 > 0. \tag{A.3}$$

Solving for the corresponding trajectory, such that $z_p(s)$ and $z_p'(s)$ remain continuous at $s = f$, gives

$$z_p(s) = \ell + \ell[1 - \cosh(\pi k(f-s)/2)]/k^2 + \ell \tan(\pi f/2) \sinh(\pi k(f-s)/2)/k. \quad \text{(A.4)}$$

Evaluating the single-chain free energy in eq. (5) and expanding in powers of f, we obtain

$$\frac{\Delta E}{k_B T} \approx \frac{\pi^6 \ell^2 (1+k^2) f^5}{320 R_0^2}. \quad \text{(A.5)}$$

The fact that $h = z_p(0) - \ell$ is then used to arrive at

$$h \approx \pi^2 \ell f^2/8, \quad \text{(A.6)}$$

which is then used to eliminate f from eq. (A.5).

This prediction can be contrasted with that of either an isolated neutral brush, where $w(z) = 0$ for $0 < z - \ell \ll h$, or two brushes in physical contact, where $w(z) = w(2\ell - z)$. With the discontinuity in the field gradient at $z = \ell$, the analogous calculation [5,6] predicts that $\Delta E \propto f^3$. This, in turn, implies that it is more costly to pull a small length of chain ($f \ll 1$) beyond the classical edge of a neutral brush as compared to that of a polyelectrolyte brush.

References

1. A.N. Semenov, Sov. Phys. JETP **61**, 733 (1985).
2. S.T. Milner, T.A. Witten, M.E. Cates, Macromolecules **21**, 2610 (1988).
3. E.B. Zhulina, O.V. Borisov, V.A. Priamitsyn, Polym. Sci. USSR **31**, 205 (1989).
4. J. Klein, E. Kumacheva, D. Mahalu, D. Perahia, L. Fetters, Nature **370**, 634 (1994).
5. S.T. Milner, T.A. Witten, Macromolecules **25**, 5495 (1992).
6. J.U. Kim, M.W. Matsen, Eur. Phys. J. E **23**, 135 (2007).
7. G.S. Grest, in *Advances in Polymer Science*, edited by S. Granick, Vol. **138** (Springer, Berlin, 1999).
8. J.B. Sokoloff, Macromolecules **40**, 4053 (2007).
9. J.B. Sokoloff, J. Chem. Phys. **129**, 014901 (2008).
10. A. Galuschko, L. Spirin, T. Kreer, A. Johner, C. Pastorino, J. Wittmer, J. Baschnagel, Langmuir **26**, 6418 (2010).
11. S.F. Edwards, Proc. Phys. Soc. London **85**, 613 (1965).
12. J.M.H.M. Scheutjens, G.J. Fleer, J. Phys. Chem. **83**, 1619 (1979).
13. C.M. Wijman, J.M.H.M. Scheutjens, Z.B. Zhulina, Macromolecules **25**, 2657 (1992).
14. M.S. Kent, L.T. Lee, B.J. Factor, F. Rondelez, G.S. Smith, J. Chem. Phys. **103**, 2320 (1995).
15. R. Baranowski, M.D. Whitmore, J. Chem. Phys. **103**, 2343 (1995).
16. M.P. Pépin, M.D. Whitmore, J. Chem. Phys. **111**, 10381 (1999).
17. M.P. Pépin, M.D. Whitmore, J. Chem. Phys. **114**, 8181 (2001).
18. J.U. Kim, M.W. Matsen, Macromolecules **42**, 3430 (2009).
19. U. Raviv, S. Glasson, N. Kampf, J.-F. Gohy, R. Jérôme, J. Klein, Nature **425**, 163 (2003).
20. U. Raviv, S. Giasson, N.Kampf, J.-F. Gohy, R. Jérôme, J. Klein, Langmuir **24**, 8678 (2008).
21. B. Liberelle, S. Giasson, Langmuir **24**, 1550 (2008).
22. I.E. Dunlop, W.H. Briscoe, S. Titmuss, M.J. Jacobs, V.L. Osborne, S. Edmondson, W.T.S. Huck, J. Klein, J. Phys. Chem. B **113**, 3947 (2009).
23. A. Naji, C. Seidel, R.R. Netz, Adv. Polym. Sci. **198**, 149 (2006).
24. M. Ballauff, O. Borisov, Curr. Opin. Colloid Interface Sci. **11**, 316 (2006).
25. P. Pincus, Macromolecules **24**, 2912 (1991).
26. R.S. Ross, P. Pincus, Macromolecules **25**, 2177 (1992).
27. O.V. Borisov, E.B. Zhulina, T.M. Birshtein, Macromolecules **27**, 4795 (1994).
28. S.J. Miklavic, S. Marcelja, J. Phys. Chem. **92**, 6718 (1988).
29. S. Misra, S. Varanasi, P.P. Varanasi, Macromolecules **22**, 4173 (1989).
30. E.B. Zhulina, O.V. Borisov, J. Chem. Phys. **107**, 5952 (1997).
31. E.B. Zhulina, J. Klein Wolterink, O.V. Borisov, Macromolecules **33**, 4945 (2000).
32. R. Israëls, F.A.M. Leermakers, G.J. Fleer, E.B. Zhulina, Macromolecules **27**, 3249 (1994).
33. E.B. Zhulina, O.V. Borisov, J. van Male, F.A.M. Leermakers, Langmuir **17**, 1277 (2001).
34. O.V. Borisov, F.A.M. Leermakers, G.J. Fleer, E.B. Zhulina, J. Chem. Phys. **114**, 7700 (2001).
35. K.N. Witte, Y.-Y. Won, Macromolecules **39**, 7757 (2006).
36. H. Seki, Y.Y. Suzuki, H. Orland, J. Phys. Soc. Jpn. **76**, 104601 (2007).
37. K.N. Witte, S. Kim, Y.-Y. Won, J. Phys. Chem. B **113**, 11076 (2009).
38. C. Seidel, Macromolecules **36**, 2536 (2003).
39. N.A. Kumar, C. Seidel, Macromolecules **38**, 9341 (2005).
40. M. Sirchabesan, S. Giasson, Langmuir **23**, 9713 (2007).
41. Q. Cao, C. Zuo, L. Li, H. He, Modell. Simul. Mater. Sci. Eng. **18**, 075001 (2010).
42. A.-C. Shi, J. Noolandi, Macromol. Theory Simul. **8**, 214 (1999).
43. Q. Wang, T. Tankashi, G.H. Fredrickson, J. Phys. Chem. B **108**, 6733 (2004).
44. M.W. Matsen, J.U. Kim, A.E. Likhtman, Eur. Phys. J. E **29**, 107 (2009).
45. R.B. Thompson, K.Ø. Rasmussen, T. Lookman, J. Chem. Phys. **120**, 31 (2004).
46. In ref. [30], the control parameters are chosen to be $\zeta \equiv H_0/\Lambda$ and $\delta \equiv d/H_0$, where $H_0 = (8N_c/3\pi^2)^{1/2} R_0$ and $\Lambda = 2R_0/L_B N_c$.
47. B.V. Derjaguin, Kolloid Z. **69**, 155 (1934).
48. N. Kampf, J.-F. Gohy, R. Jérôme, J. Klein, J. Polym. Sci. Part B **43**, 193 (2005).